Journal of Applied Electrochemistry **32**: 359–367, 2002.

Preparation of CdS thin films by electrodeposition: effect of colloidal sulfur particle stability on film composition

M. TAKAHASHI[1]*, S. HASEGAWA[1], M. WATANABE[1], T. MIYUKI[2], S. IKEDA[2] and K. IIDA[3]
[1]*Department of Industrial Chemistry, Chubu University, Matsumoto-cho 1200, Kasugai, Aichi 487-8501, Japan*
[2]*Department of Applied Chemistry, Nagoya Institute of Technology, Gokiso-cho, Showa-ku, Nagoya, Aichi 466-8555, Japan*
[3]*Nagoya Municipal Industrial Research Institute, 4-41 Rokuban, 3-chome, Atsuta-ku, Nagoya, Aichi 456 Japan*
*(*author for correspondence, e-mail: thinfilm@isc.chubu.ac.jp)*

Received 13 February 2001; accepted in revised form 6 February 2002

Key words: CdS thin film, electrodeposition, protective colloid, XPS

Abstract

CdS thin films of about 1 μm thickness were deposited from an aqueous solution containing Cd^{2+}, $Na_2S_2O_3$ and gelatin as the protective colloid to stabilize the size of colloidal sulfur at from 30 to 40 nm and keep the concentration to an appropriate value during electrolysis. The effects of concentrations of Cd^{2+} and $S_2O_3^{2-}$ ions and the deposition potential on the composition of CdS films were studied. The reaction mechanism of CdS film formation on the electrode is discussed. CdS film, whose composition is uniform across the film and which does not contain excess metallic cadmium, can be deposited from a solution containing 0.50 to 2.00 mM $Cd(NO_3)_2$, 1.00 to 5.00 mM $Na_2S_2O_3$ and 1.0×10^{-7} to 1.0×10^{-3} wt % gelatin.

1. Introduction

Cadmium sulfide (CdS) is one of the most attractive semiconductors for use in solar cells [1–4], photoconducting sensors [5] and Cd^{2+} ion selective sensors [6]. CdS thin films are generally produced using various techniques such as chemical vapour deposition [7] and chemical bath deposition [8]. They can also be deposited electrochemically from aqueous [9–13] or organic solutions [14–17]. Although many papers on electrodeposition of CdS thin films have been published, two major problems remain. When CdS films are deposited from an aqueous solution containing Cd^{2+} and $Na_2S_2O_3$, the problem is that the CdS formation reaction on the electrode is not clear. The following formation reactions for the CdS electrodeposition are proposed:

$$\text{(Type 1)}\ Cd^{2+} + S\ (\text{colloid}) + 2e^- \rightarrow CdS \qquad (1a)$$

$$\text{(Type 2)}\ S + 2e^- \rightarrow S^{2-}, \qquad Cd^{2+} + S^{2-} \rightarrow CdS \qquad (1b)$$

$$\text{(Type 3)}\ Cd^{2+} + 2e^- \rightarrow Cd, \qquad Cd + S \rightarrow CdS \qquad (1c)$$

The other problem is that excess metallic cadmium exists in the electrodeposited CdS films. To solve this, Fatas et al. [18] proposed the use of a pulse potential technique. In this method, a film containing CdS and excess Cd metal is formed at the cathodic potential, and the excess Cd metal in the film is removed by anodic dissolution. However, it is difficult to maintain an optimal potential.

We consider that these problems originate in the source of sulfur used in the electrodeposition. In the electrodeposition of CdS films, the colloidal sulfur into which $S_2O_3^{2-}$ is decomposed is generally used, and it is well known that colloidal sulfur particles grow with time by interaction with $S_2O_3^{2-}$ anions [19]. When larger than a critical particle size, these sulfur particles settle and cannot take part in the electrode reaction. Consequently, the composition of electrodeposited CdS films includes considerable excess Cd metal.

By supposing the growth of the colloidal sulfur particles to be hindered, we reasoned that concentration in the electrolytic solution would remain the same. Thus, we attempted to add a protective colloid to the electrolytic solution so that the colloidal sulfur particles are stabilized at an appropriate size, and the changes in the colloidal sulfur particle concentration maintain a certain value during the electrolysis. We report the effect of Cd^{2+} ion concentration, $S_2O_3^{2-}$ concentration, and deposition potential on the composition of electrodeposited CdS films and discuss the formation reaction of CdS on the electrode.

2. Experimental details

It is known that the growth of colloidal particles is strongly affected by the preparation method. Electrolytic solutions were prepared by the procedure represented in Figure 1. Reagent grade HNO_3, $Cd(NO_3)_2$ (purity 99%), $Na_2S_2O_3$ (purity 99.5%) and gelatin were used without further purification. Water was purified by the Milli-Q water purification system (Millipore Corporation). The CdS films were deposited from acidic solutions of pH 2.1 ± 0.1 containing various concentrations of $Cd(NO_3)_2$, $Na_2S_2O_3$ and gelatin on Ti sheets (Nilaco Co.) which were decreased by chloroform and ethanol in an ultrasonic cleaner for 10 min and washed in purified water before use. The usual three-electrode cell was used for the preparation of CdS films. A platinum wire and a Ag/AgCl electrode were employed as a counter electrode and a reference electrode, respectively. A Hokuto Denko HAB-151 potentiostat instrument was used for the potentiostatic deposition of CdS films (film thickness about 1 μm). The electrodeposition was carried out at room temperature after the electrolytic solutions were deaerated by passing Ar gas through them for about 15 min. The structure of the electrodeposited films was studied using a Rigaku Denki RAD-1B X-ray diffractometer with a copper target. The composition and oxidation state of the films were investigated using a Shimadzu ESCA 3300 system. The microstructure and composition of the films were examined using an Akashi scanning electron microscope (SEM) DS-130 equipped with EDS. The correction for the composition obtained by ESCA (XPS) and EDS measurements was made using the calibration curve for the Cd element made by the Cd–CdS standard mixtures. The turbidity of the solution was measured at 550 nm using a Shimadzu UV-2500 reflect meter. The size distribution of the colloidal sulfur in the electrolytic solution was measured by a Nicomp 370 laser particle analyser system. The microstructure and diameter of the colloidal sulfur particles were measured using a JEOL transmission electron microscope (TEM) 2010. The colloidal sulfur particles were dispersed in chloroform by ultrasonic blending, and the resulting suspension was applied in a drop-wise manner to the carbon filter of a metal grid. The grid was then placed within the TEM operating at 200 kV. The reflection spectra of the films were recorded by a Shimadzu UV-2500 reflect meter.

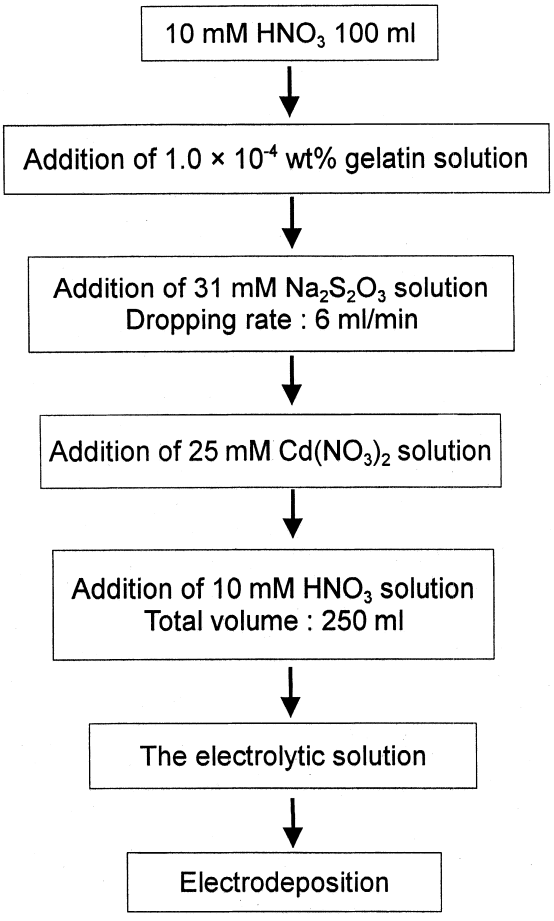

Fig. 1. Preparation of the electrolytic solution.

3. Results

3.1. *Stabilization and size distribution of colloidal sulfur*

The time dependence of the turbidity of the electrolytic solution is shown in Figure 2. The plot (▲) depicts the time dependence of the turbidity obtained for an acidic solution (pH = 2.10) containing 5.00 mM $Na_2S_2O_3$ and 0 wt % gelatin. The turbidity rapidly increases with an increase in time and this solution shows the characteristic turbidity of colloidal sulfur. That turbidity has a maximum value near 25 min and decreases with time. Then the colloidal sulfur particles begin to precipitate and the clarity of the solution begins to increase. For the solution containing 5.00 mM $Na_2S_2O_3$ and 1.0×10^{-5} wt % gelatin (plot (●)), the turbidity increases with time and stabilizes after 30 min. In this solution the precipitation of colloidal sulfur particles is not observed, and when the concentration of $Na_2S_2O_3$ is less than

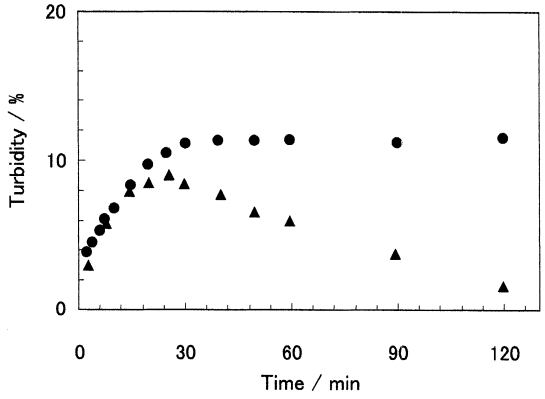

Fig. 2. Turbidity–time profiles of electrolytic solutions containing 5.00 mM $Na_2S_2O_3$, (▲) 0 wt % gelatin and (●) 1.0×10^{-5} wt % gelatin.

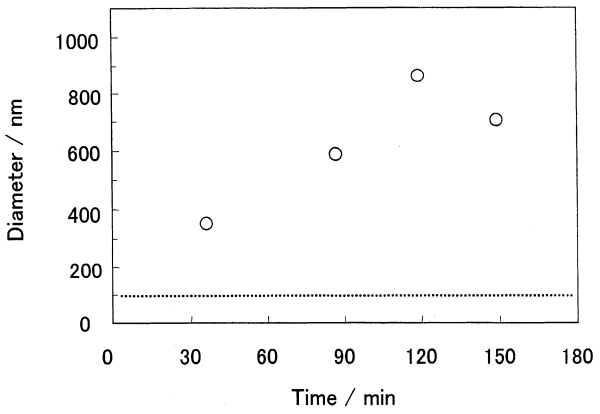

Fig. 3. Average diameter of sulfur particles as a function of time. Acidic solutions (pH = 2.1) containing 1.0 mM $Na_2S_2O_3$ and various concentrations of gelatin: (a) 0 wt %, (b) 1.0×10^{-5} wt %.

2.0 mM and the concentration of gelatin is 1.0×10^{-5} wt %, the solution is colorless and transparent, and the turbidity is not measurable.

The size distribution of colloidal sulfur in the solution containing 1.00 mM $Na_2S_2O_3$ and various concentrations of gelatin were measured. The result for the solution containing no gelatin indicates that the shape of the measured size distribution shows a good Maxwell–Boltzmann distribution with the mean diameter of the sulfur particle at 969 nm, (that diameter as a function of time is shown in Figure 3). On the one hand in the solution containing 1.0 mM $Na_2S_2O_3$ and 0 wt % gelatin, the diameter of the sulfur particles increases with time, reaching a maximum value at 120 min. The diameter decreases with time because the large particles (>1.0 μm) settle out of the solution and the smaller particles remain. On the other hand, in the solution containing 1.00 mM $Na_2S_2O_3$ and 1.0×10^{-5} wt % gelatin, the size distribution could not be measured by our laser-particle analyser system, and particle growth could not be observed for up to 48 h. However when a He–Ne laser beam passes through this solution in the darkroom, the Tyndal phenomenon is observed clearly. These results indicate that the sulfur particle size is smaller than 100 nm, which is the minimum value measurable by our apparatus.

The TEM micrograph and the diffraction pattern of the sulfur particles prepared from the solution containing 1.00 mM $Na_2S_2O_3$ and 1.0×10^{-5} wt % gelatin are shown in Figure 4. In Figure 4(a), the crystal lattices are observed in the particles, and the spacing of the lattice planes is about 390 pm (picometer). The average grain size of the particles is 40 ± 10 nm. In the electron diffraction pattern (Figure 4(b)), many diffraction spots and Debye–Scherrer rings are observed. The brightest ring is due to the diffraction of the carbon filter, and the distance from the centre to the ring is 350 pm. An analysis of the diffraction pattern confirmed that this particle is rhombic sulfur, which consists of S_8 compounds, and that the lattice planes observed in Figure 4(a) correspond to the crystal face (1 0 1) with a spacing at 385 pm.

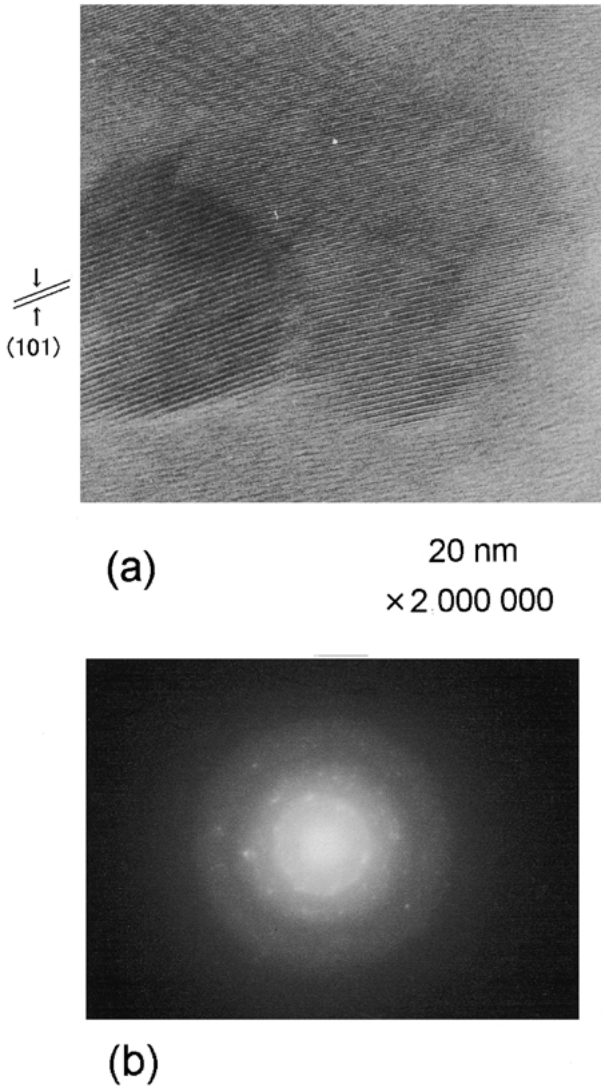

Fig. 4. High resolution TEM micrograph (a), including electron diffraction pattern (b), of sulfur particles prepared from the solution containing 1.00 mM $Na_2S_2O_3$ and 1.0×10^{-5} wt % gelatin.

From the results described above, we conclude that, in the CdS formation reaction, the reactant of sulfur is the very small rhombic sulfur particle rather than amorphous or atomic sulfur and that the addition of the gelatin can stabilize the size and density of the colloidal sulfur particles in the solution.

3.2. *Voltammogram*

Voltammograms were used to determine the electrodeposition mechanism of CdS films. The voltammograms obtained in solutions containing 0.50 mM $Cd(NO_3)_2$, 1.0×10^{-5} wt % gelatin and various concentrations of $Na_2S_2O_3$ are shown in Figure 5. In Figure 5(a) depicting the solution containing 1.00 mM $Na_2S_2O_3$, the cathodic current is observed to flow at potentials more negative than −0.60 V, and a light yellow film forms on the electrode. In this voltammogram one cathodic current peak is observed at −1.22 V. In Figure 5(b) giving the solution containing 5.00 mM $Na_2S_2O_3$, the cathodic

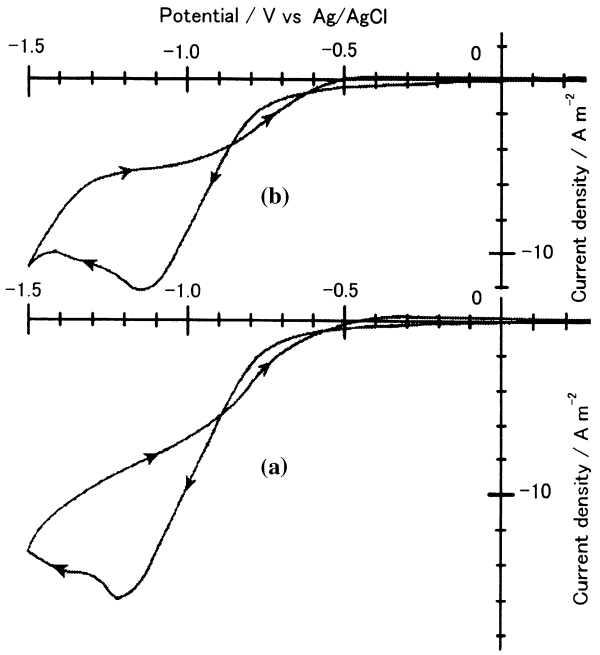

Fig. 5. Influence of $Na_2S_2O_3$ concentration on voltammograms. Acidic solution (pH = 1.2) contains 0.50 mM $Cd(NO_3)_2$, 1.0×10^{-5} wt % gelatin and (a) 1.00 mM $Na_2S_2O_3$ and (b) 5.00 mM $Na_2S_2O_3$.

current flows at potentials more negative than −0.60 V and a light yellow film forms on the electrode, with one cathodic current peak observed at −1.15 V. The dependence of the cathodic peak current density (I_p) on $Na_2S_2O_3$ concentration is shown in Figure 6. That density is independent of $Na_2S_2O_3$ concentration up to 5.00 mM, and those values are constant at -10.8 ± 0.5 A m^{-2}. However, above 5.00 mM $Na_2S_2O_3$, the cathodic peak current density decreases with an increase in the $Na_2S_2O_3$ concentration. The dependence of the cathodic peak potential (E_p) and the decomposition potential (E_d) on $Na_2S_2O_3$ concentration is shown in

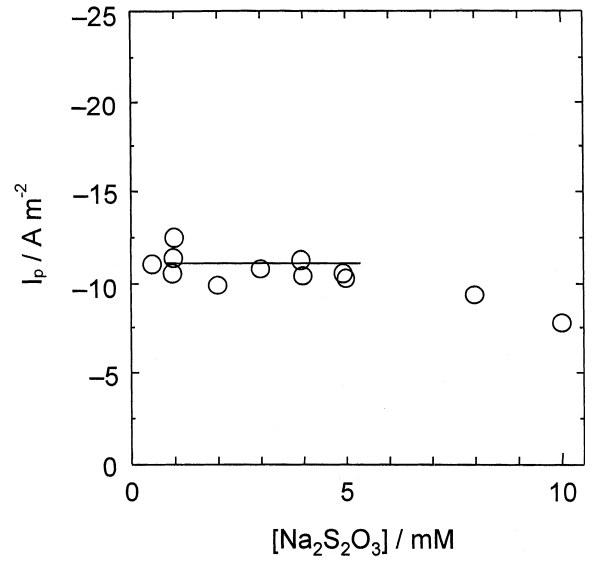

Fig. 6. Dependence of the cathodic peak current density on $Na_2S_2O_3$ concentration. Other conditions are the same as those in Figure 5.

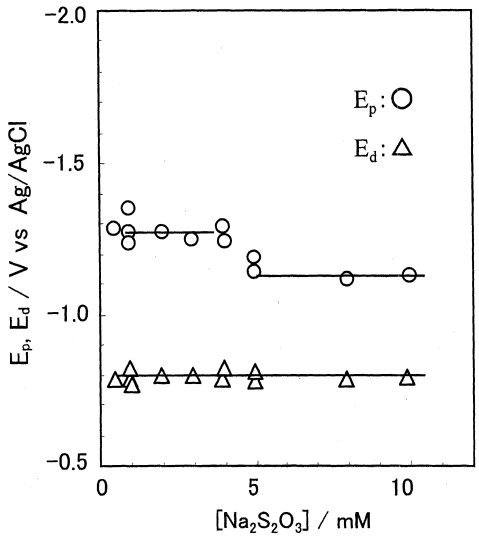

Fig. 7. Dependence of the cathodic peak potential (E_p) and decomposition potential (E_d) on $Na_2S_2O_3$ concentration.

Figure 7. These results show that all decomposition potentials are near −0.79 V and are independent of $Na_2S_2O_3$ concentration. The cathodic peak potentials observed for solutions containing $Na_2S_2O_3$ less than 4.00 mM are near −1.27 V and are independent of $Na_2S_2O_3$ concentration. However, when the concentration of $Na_2S_2O_3$ is above 5.00 mM, peak potentials shift toward the positive potential near −1.13 V, and I_p and E_p shift with an increase in $Na_2S_2O_3$ concentration. These results can be explained as follows. When the $Na_2S_2O_3$ concentration is above 5.00 mM, the shape of the size distribution does not show a Maxwell–Boltzmann distribution and colloidal sulfur particles are divided into two classes. Class 1 consists of sulfur particles that can take part in the electrode reaction, and class 2 is comprised of sulfur particles that do not participate in the electrode reaction. Class 1 sulfur particles are expected to be more reactive than those in class 2, but their concentration is lower. Moreover, the mean particle size in class 1 is larger than 40 nm, so that its diffusion coefficient becomes small, and E_p shifts in the direction of the positive potential and I_p decreases.

The voltammograms measured in the solutions containing 1.00 mM $Na_2S_2O_3$, 1.0×10^{-5} wt % gelatin and various concentrations of $Cd(NO_3)_2$ are shown in Figure 8. In Figure 8(a) denoting the solution containing 1.00 mM $Cd(NO_3)_2$, the cathodic current is observed to flow at potentials more negative than −0.59 V, and light yellow film forms on the electrode. In this voltammogram one cathodic current peak (peak I) is observed at −1.27 V. For the solution containing 5.00 mM $Cd(NO_3)_2$ (see Figure 8(b)), a cathodic current is observed to flow at potentials more negative than −0.50 V, and a gray film forms on the electrode. Two cathodic current peaks are observed at −0.92 V and −1.29 V, and two anodic current peaks are observed at −0.33 V and −0.20 V. The cathodic current peak at −0.92 V (peak II) and the two anodic current peaks are

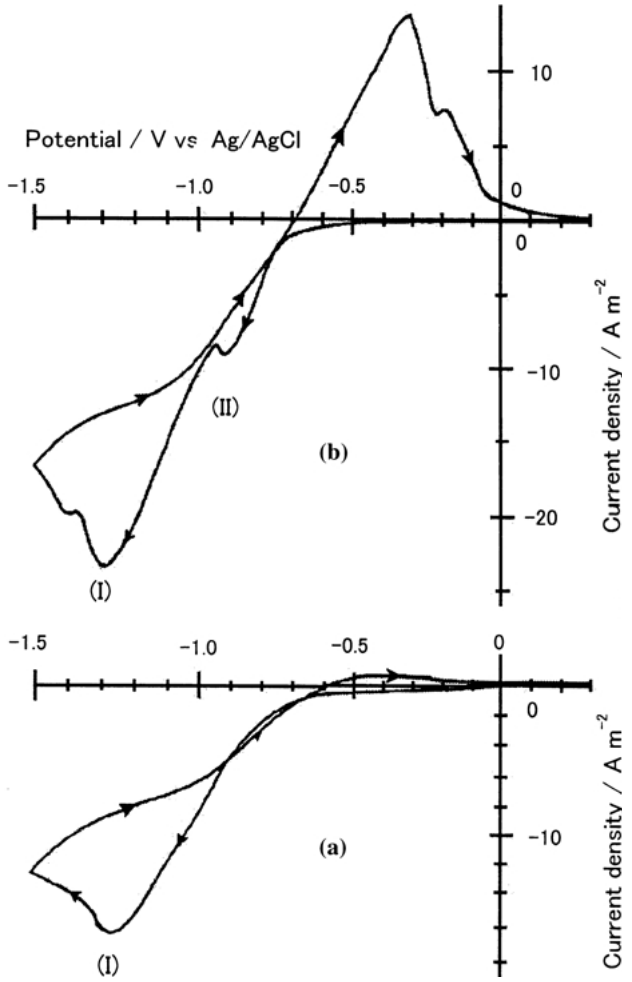

Fig. 8. Influence of $Cd(NO_3)_2$ concentration on voltammograms. Acidic solution (pH = 1.2) contains 1.00 mM $Na_2S_2O_3$, 1.0×10^{-5} wt % gelatin and (a) 1.00 mM $Cd(NO_3)_2$ and (b) 5.00 mM $Cd(NO_3)_2$.

found only in solutions containing $Cd(NO_3)_2$ of more than 2.00 mM. The dependence of two cathodic peak current densities on $Cd(NO_3)_2$ concentration is shown in Figure 9. These two peak current densities are proportional to the $Cd(NO_3)_2$ concentration, though a dependence of the peak current on $Na_2S_2O_3$ concentration was not observed in Figure 6. The dependence of the two cathodic peak potentials and the decomposition potential on $Cd(NO_3)_2$ concentration is shown in Figure 10. The potentials of peak I do not depend on $Cd(NO_3)_2$ concentration. This result agrees with that depicted in Figure 7. The potentials of peak II depend on the $Cd(NO_3)_2$ concentration and the positions move toward the negative potential with an increase in $Cd(NO_3)_2$ concentration. This result may be explained as follows. The composition of films changes with solution composition, so the electron transfer rate of the Cd^{2+} reducing reaction from Cd^{2+} to Cd metal is thereby changed. When peak II is not observed in the voltammogram, the decomposition potential is independent of $Cd(NO_3)_2$ concentration and is near −0.79 V. On the other hand when peak II is observed, the decomposition potential shifts toward the positive

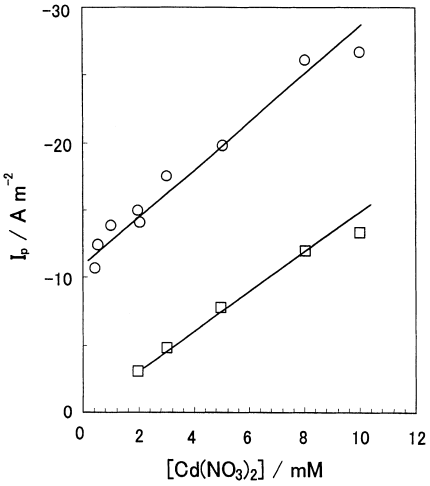

Fig. 9. Dependence of the cathodic peak current density on $Cd(NO_3)_2$ concentration. Key: (○) cathodic peak I; (□) cathodic peak II. Other conditions are the same as those in Figure 8.

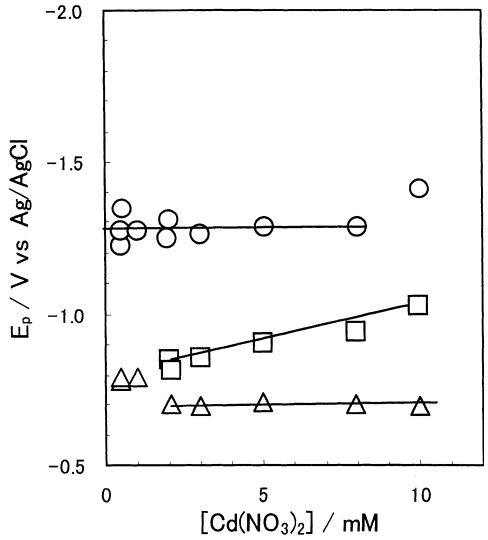

Fig. 10. Dependence of the cathodic peak potential (E_p) and decomposition potential (E_d) on $Cd(NO_3)_2$ concentration. Key: (○) cathodic peak I, (□) cathodic peak II, (△) decomposition peak.

potential and is near −0.69 V. This decomposition potential of −0.69 V agrees with the starting potential of the Cd^{2+} reducing reaction ($Cd^{2+} + 2e^- \rightarrow Cd$). Therefore, we consider that the peak II corresponds to the reducing reaction ($Cd^{2+} + 2e^- \rightarrow Cd$).

3.3. *X-ray diffraction patterns of electrodeposited films*

The X-ray diffraction patterns of the films deposited at −1.10 V vs Ag/AgCl in the solutions containing 0.50 mM $Cd(NO_3)_2$, 1.00 mM $Na_2S_2O_3$, and (a) 0 wt % gelatin and (b) 1.0×10^{-5} wt % gelatin are shown in Figure 11. In Figure 11(a) diffraction peaks are observed at $2\theta = 31.8$, 34.7, 38.3, and 47.8°, and these peaks correspond to the (0 0 2), (1 0 0), (1 0 1), and (1 0 2) faces of Cd metal [20], respectively. The films deposited from the solutions not containing gelatin are silver–gray, and it is

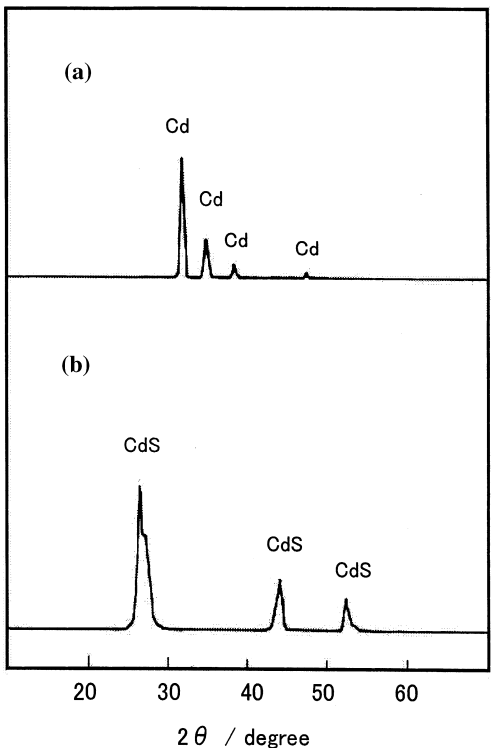

Fig. 11. X-ray diffraction patterns of films deposited from the acidic solution (pH 2.1) containing 0.50 mM $Cd(NO_3)_2$, 1.0 mM $Na_2S_2O_3$, and various concentrations of gelatin: (a) 0 wt %, (b) 1.0×10^{-5} wt %. Deposition potential −1.10 V vs Ag/AgCl.

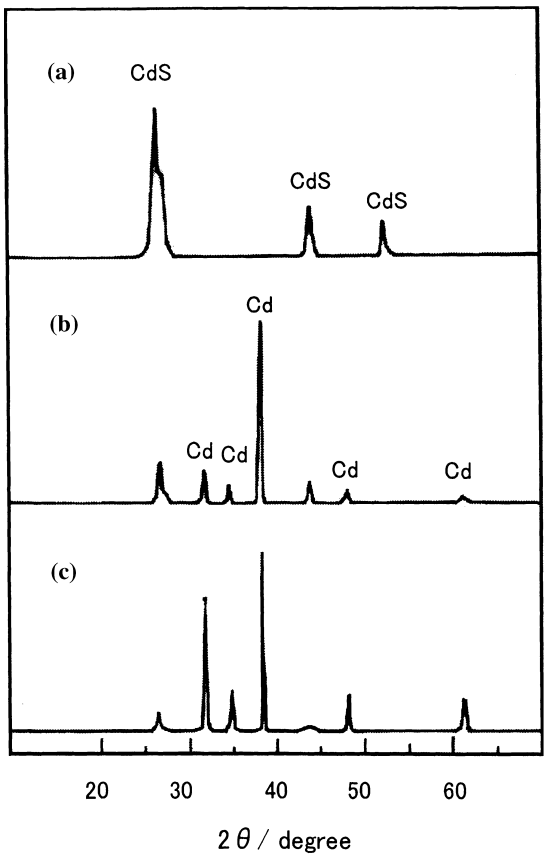

Fig. 12. X-ray diffraction patterns of films deposited from the acidic solution (pH 2.1) containing 1.0 mM $Na_2S_2O_3$, 1.0×10^{-5} wt % gelatin, and various concentrations of $Cd(NO_3)_2$: (a) 0.50 mM, (b) 2.00 mM, (c) 5.00 mM. Deposition potential was −1.10 V vs Ag/AgCl.

difficult to observe the diffraction peaks of CdS. It is suggested that this film deposited from the solution not containing gelatin mainly consists of Cd metal. On the other hand, in Figure 11(b) the broad and weak diffraction peaks are observed at $2\theta = 26.5$, 43.9, and 52.2°, and these peaks correspond to the (1 1 1), (2 2 0), and (3 1 1) faces of cubic CdS [21], respectively. The films deposited from the solution containing 1.0×10^{-5} wt % gelatin are yellow, and the diffraction peaks of Cd metal are not observed in these films. The same results are also obtained for the CdS films deposited from solutions containing 1×10^{-7} and 1×10^{-3} wt % gelatin. We measured X-ray diffraction patterns of the films deposited at −1.10 V vs Ag/AgCl in the solutions containing 0.50 mM $Cd(NO_3)_2$, 1.0×10^{-5} wt % gelatin and various concentrations of $Na_2S_2O_3$ in the range from 0.50 to 10.0 mM. In all diffraction patterns, the broad and weak diffraction peaks corresponding to (1 1 1), (2 2 0) and (3 1 1) faces of cubic CdS, respectively, were observed, and the diffraction peaks due to excess sulfur and metallic Cd were not.

The X-ray diffraction patterns of films deposited at −1.10 V in the solution containing 1.0 mM $Na_2S_2O_3$, 1.0×10^{-5} wt % gelatin, and various concentrations of $Cd(NO_3)_2$ are shown in Figure 12. In Figure 12(a), for film deposited in the solution containing 0.5 mM $Cd(NO_3)_2$, the broad and weak diffraction peaks due to CdS are observed at $2\theta = 26.5$, 43.9, and 52.2°. In Figure 12(b), for film deposited in the solution containing 2.0 mM $Cd(NO_3)_2$, the new diffraction peaks due to Cd metal are observed at $2\theta = 31.8$, 34.7, 38.3 and 47.8°. The intensities of these Cd metal diffraction peaks increase with an increase in $Cd(NO_3)_2$ concentration in the solution.

The X-ray diffraction patterns of films deposited at various potentials in the solution mentioned in Figure 12(a) are shown in Figure 13. When the films are deposited at the potential in the region of −0.80 to −1.40 V, only these diffraction peaks due to CdS are observed. The products are independent of the deposition potential in the region from −0.80 to −1.40 V and depend on the composition of the solution. When the deposition potential is in the range from −0.60 to −0.80 V, though the deposition rate is very slow, only the diffraction peaks due to CdS are observed. On the other hand, when the deposition potential is more negative than −1.40 V, many bubbles are formed on the electrode surface, and a very thin yellow film is deposited on the electrode, but the diffraction pattern of this film cannot be measured.

3.4. *XPS measurements*

The XPS spectra of film deposited under the conditions mentioned in Figure 11(b) are shown in Figure 14. When Figure 14(a) is observed in a wide scan range, the

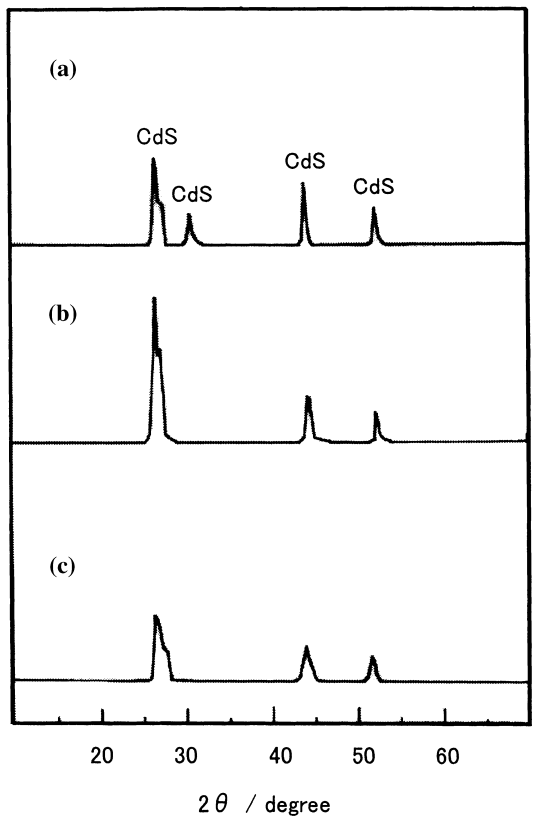

Fig. 13. X-ray diffraction patterns of films deposited from the acidic solution (pH 2.1) containing 0.50 mM $Cd(NO_3)_2$, 1.0 mM $Na_2S_2O_3$ and 1.0×10^{-5} wt %. Deposition potentials: (a) −0.80 V, (b) −1.10 V and (c) −1.40 V vs Ag/AgCl.

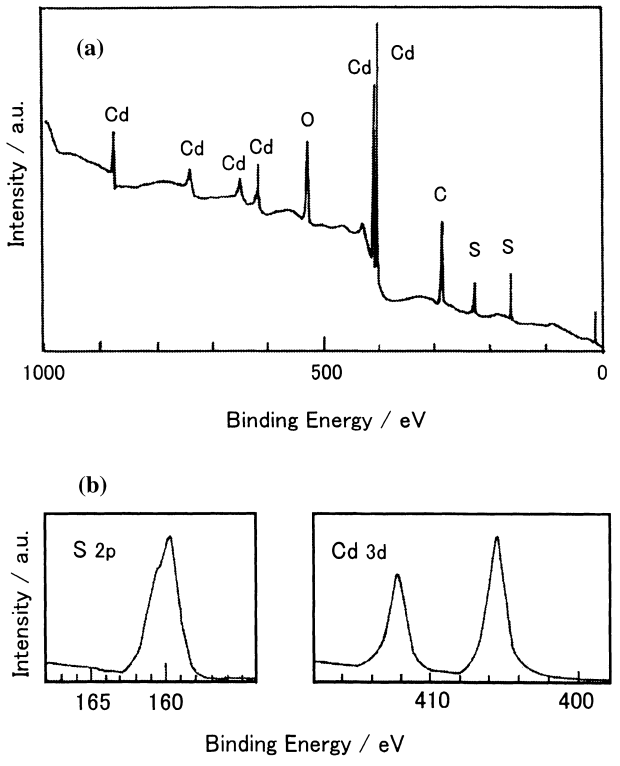

Fig. 14. XPS spectra of the CdS film deposited under conditions mentioned in Figure 11(b). (a) wide scan, (b) narrow scan of Cd 3d and S 2p.

absence of peaks corresponding to the substrate (mainly the Ti peak) is noteworthy. This indicates full coverage of the substrate by a compact film. In Figure 14(b), which depicts the region S 2p and Cd 3d peaks, the peaks corresponding to S^{2-} are only observed at 161.0 and 160.0 eV [22] and those corresponding to S or SO_4^{2-} are absent. The peaks observed at 412.5 and 405.8 eV correspond to Cd^{2+} [19]. The ratio of the S 2p peaks area to Cd 3d peaks area is 0.092, and this value agrees with the value 0.095 ± 0.007 of a standard CdS sample (purity 99.999%) within the experimental error. The average concentrations of Cd and S in this film were also determined by EDX measurements, and it was found that the Cd concentration was 48 ± 4 at % and that the S concentration was 52 ± 5 at %. These values agree well with the values observed in EDX measurements of a standard CdS sample. And XPS depth profile of this CdS film was measured. The result indicated that the ratio of S to Cd in the film was 0.092 ± 0.002, and that the film composition was constant in the thickness direction. The same results were also obtained from XPS measurements of the CdS films electrodeposited from the solution containing 1.0×10^{-5} and 1.0×10^{-3} wt % gelatin.

Figure 15 shows the relations between film composition and the $Cd(NO_3)_2$ and $Na_2S_2O_3$ levels. These results establish that the composition of films is independent of the $Na_2S_2O_3$ concentration, and that the ratio of the S peak area to the Cd peak area is 0.095 ± 0.008. With $Cd(NO_3)_2$, the film composition is constant ($A(S)/A(Cd) = 0.095$) up to 2 mM $Cd(NO_3)_2$, and when the $Cd(NO_3)_2$ concentration exceeds 2 mM, the concentration of the Cd element in the films increases with an increasing $Cd(NO_3)_2$ concentration in the solution.

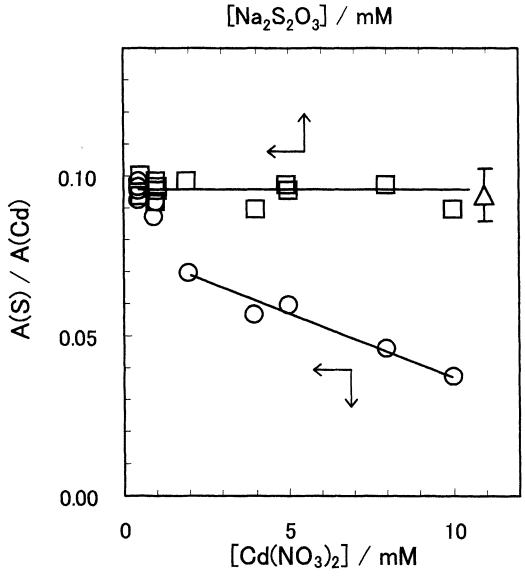

Fig. 15. Ratio of XPS peak areas corresponding to Cd 3d and S 2p as a function of $Na_2S_2O_3$ (□) and $Cd(NO_3)_2$ (○) concentration. Deposition condition: (□) 0.50 mM $Cd(NO_3)_2$, (○) 1.00 mM $Na_2S_2O_3$, 1.0×10^{-5} wt % gelatin. Deposition potential −1.10 V vs Ag/AgCl.

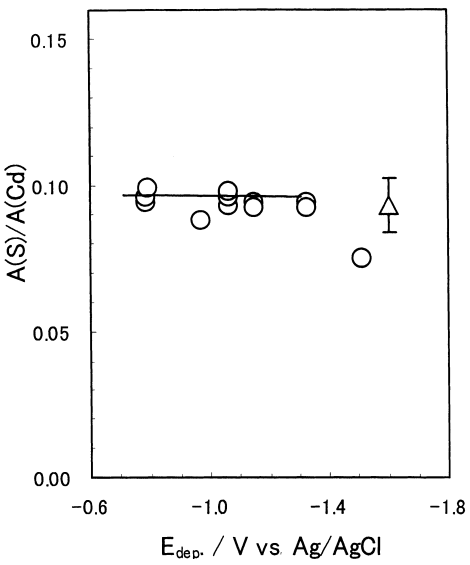

Fig. 16. Ratio of XPS peak areas corresponding to Cd 3d and S 2p as a function of deposition potential. Deposition condition: 0.50 mM $Cd(NO_3)_2$, 1.00 mM $Na_2S_2O_3$, 1.0×10^{-5} wt % gelatin.

The relations between the composition of films deposited in the solution containing 0.50 mM $Cd(NO_3)_2$ and 1.00 mM $Na_2S_2O_4$ and the deposition potentials are shown in Figure 16. In the potential region of −0.80 to −1.40 V, the composition of the films is found to be independent of the deposition potentials. When the films are deposited at a potential more negative than −1.40 V or more positive than −0.80 V, the films are so thin that XPS measurements can not be made.

The reflection spectrum of the above mentioned sample deposited from the solution containing 1.0×10^{-5} wt % gelatin has been studied in the wavelength range of 350–850 nm at room temperature and is shown in Figure 17. The reflectance changes rapidly in the range of 490–550 nm. The bandgap energy determined from the spectrum is about 2.38 eV, and this is in good agreement with the value of 2.42 eV reported for CdS single crystals.

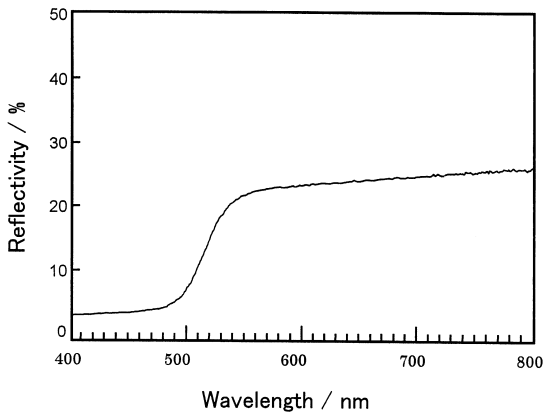

Fig. 17. Diffuse reflection spectrum of electrodeposited CdS film. Deposition conditions are the same as those in Figure 11(b).

4. Discussion

The basic results can be summarized as follows:

(i) Gelatin prevents the growth and sedimentation of sulfur particles and stabilizes colloidal sulfur at the small particle size (about 30–40 nm).
(ii) The colloidal sulfur particle is not amorphous, and consists of rhombic sulfur composed of S_8 molecules.
(iii) The CdS film whose composition is uniform across the film and which does not contain excess metallic cadmium can be deposited from a solution containing 0.50–2.00 mM $Cd(NO_3)_2$, 1.00–5.00 mM $Na_2S_2O_3$, and $1.0 \times 10^{-7} - 1.0 \times 10^{-3}$ wt % gelatin.
(iv) The cathodic current density of CdS formation depends on the Cd^{2+} concentration rather than the $S_2O_3^{2-}$ concentration.
(v) When the decomposition potential is near −0.80 V, the CdS films that do not contain excess metallic cadmium can be deposited in the potential range from −0.80 to −1.40 V.

The formation mechanism of CdS films can be explained as follows. The $S_2O_3^{2-}$ ion is unstable in acidic media (pH < 4.0) and decomposes into sulfur (S) and $S_2O_3^{2-}$ ion according to the following equation:

$$S_2O_3^{2-} \rightarrow (S) + S_2O_3^{2-} \tag{2}$$

This sulfur (S) becomes the nucleus of crystal growth, and the decomposition of $S_2O_3^{2-}$ takes place on its surface, causing the sulfur particle to grow. At the electrode surface, the sulfur particle reacts with Cd^{2+} ion and electrons to give

$$8\ Cd^{2+} + S_8 + 16\ e^- \rightarrow 8\ CdS \tag{3}$$

This overall CdS formation reaction agrees with that proposed by Baranski et al. [23]. They undertook the electrodeposition of CdS films in a diethylene glycol (DEG) solution containing cadmium perchlorate and elemental sulfur (rhombic sulfur), and reported that the formation mechanism of CdS films involves the following series of reactions:

$$S_8 + 2\ e^- \rightarrow (S_8^{2-})_{ads} \quad \text{slow} \tag{4}$$

$$Cd^{2+} + (S_8^{2-})_{ads} \rightarrow CdS + S_7 \quad \text{fast} \tag{5}$$

$$S_7 + 2\ e^- \rightarrow (S_7^{2-})_{ads} \quad \text{fast} \tag{6}$$

$$Cd^{2+} + (S_7^{2-})_{ads} \rightarrow CdS + S_6 \quad \text{fast} \tag{7}$$

In these equations, S_8 is a component of rhombic sulfur. The type 2 formation mechanism mentioned in the introduction (Section 1) is due to this mechanism in which the rate-determining step is Equation 4.

As mentioned above, in our experiments the CdS formation current does not depend on the concentration of colloidal sulfur particles that depend on the $S_2O_3^{2-}$ concentration in the solution, but rather on the Cd^{2+} concentration, and the rhombic sulfur stoichiometric CdS films can be made on the condition that the ratio of the Cd^{2+} concentration to the $S_2O_3^{2-}$ concentration in the solution is smaller than 1. In addition, it is well known that colloidal sulfur particles are specifically adsorbed on the metal surface and that the cation is adsorbed on the sulfur colloid because it is negative colloid. Therefore, CdS formation reactions are expressed by the following equations:

$$S_8 \rightarrow S_{8ads} \quad \text{fast (specific adsorption)} \tag{8}$$

$$^{*}Cd^{2+} + S_{8ads} + 2e^{-} \rightarrow CdS + S_{7ads} \quad \text{slow (rate determining step)} \tag{9}$$

$$^{*}Cd^{2+} + S_{7ads} + 2e^{-} \rightarrow CdS + S_{6ads} \quad \text{fast} \tag{10}$$

$$^{*}Cd^{2+} + S_{6ads} + 2e^{-} \rightarrow CdS + S_{5ads} \quad \text{fast} \tag{11}$$

where $^{*}Cd^{2+}$ is expressed as the Cd^{2+} cation that is in the solution or adsorbed on the sulfur colloid.

In the first step, the small sulfur particles, on which some Cd^{2+} cations are adsorbed, are adsorbed on the electrode. In the second step, the S_8 species and the Cd^{2+} cation adsorbed on the sulfur particle interact, and CdS is formed. This second step is the rate-determining step of CdS electrodeposition. In the third step, other sulfur species containing less than eight sulfur atoms and Cd^{2+} ion interact and CdS is formed.

Therefore, when gelatin is added to the electrolytic solution, it inhibits the growth of the sulfur particles and stabilizes the colloidal sulfur particles so that the number of small sulfur particles reaching the electrode surface per unit time seems almost constant during the electrodeposition of CdS film, and the CdS formation reaction continues during electrodeposition. Consequently, the composition of the CdS films electrodeposited from the solution to which gelatin was added becomes constant in the thickness direction. If gelatin is not added to the solution, the number of sulfur particles reaching the electrode surface per unit time decreases with the deposition time, and the reduction of the metallic cadmium takes precedence over the CdS formation reaction. As a result, the composition of film electrodeposited from the solution not containing gelatin changes in the thickness direction, and excess metallic cadmium is formed in the electrodeposited CdS film.

Acknowledgements

This work was partially supported by Grants-in-Aid for Scientific Research on Priority Area of Electrochemistry of Ordered Interfaces (no. 09237101).

References

1. S. Wagner, J.L. Shay, K.J. Bachmann and E. Buehler, *Appl. Phys. Lett.* **26** (1975) 229.
2. K. Mitchell, A.L. Fahrenbruch and R.H. Bube, *J. Appl. Phys.* **48** (1977) etc. 4365.
3. K. Yamaguchi, N. Nakayama, H. Matsumoto and S. Ikegami, *Jpn. J. Appl. Phys.* **16** (1977) 1203.
4. L.C. Isett, *J. Appl. Phys.* **55** (1984) 3190.
5. N.R. Pavaskar, C.A. Menezes and A.P.B. Sinha, *J. Electrochem. Soc.* **124** (1977) 743.
6. H. Hirata and K. Higashiyama, *Fresenius' Z. Anal. Chem.* **257** (1971) 104.
7. M. Bettini, K.J. Bachmann and E. Buehler, *J. Appl. Phys.* **48** (1977) 1603.
8. J. Humenberger, G. Linnert and K. Lischka, *Thin Solid Films* **121** (1984) 75.
9. G.P. Power, D.R. Peggs and A.J. Parker, *Electrochim. Acta* **26** (1981) 681.
10. J.F. McCann and M.S. Kazacos, *J. Electroanal. Chem.* **119** (1981) 409.
11. B.M. Basol, *Solar Cells* **23** (1988) 69.
12. S.K. Das and G.C. Morris, *Solar Energy Materials and Solar Cells* **28** (1993) 305.
13. B.E. McCandal, A. Mondal and R.W. Birkmire, *Solar Energy Materials and Solar Cells* **36** (1995) 369.
14. E. Fatas, P. Herrasti, F. Arjona, E.G. Camarero and J.A. Medina, *Electrochim. Acta* **32** (1987) 139.
15. E. Fatas and P. Herrasti, *Electrochim. Acta* **33** (1988) 959.
16. S. Preusser and M. Cocivera, *J. Electroanal. Chem.* **252** (1988) 139.
17. R. Flood, B. Enright, M. Allen, S. Barry, A. Dalton, H. Doyle, D. Tynan and D. Fitzmaurice, *Solar Energy Materials and Solar Cells* **39** (1995) 83.
18. E. Fatas, P. Herrasti, F. Arjona and E.G. Camarero, *J. Electrochem. Soc.* **134** (1987) 2799.
19. E.M. Zaiser and V.K. La Mer, *J. Colloid Sci.* **3** (1948) 571.
20. ASTM X-Ray Powder Data 5–674.
21. ASTM X-Ray Powder Data 22–829.
22. K. Siegbahn, C. Nordling, A. Fahlman, R. Nordberg, K. Harmrin, J. Hadman, G. Johansson, T. Bergmark, S.E. Karlsson, I. Lindgren and B. Lindberg, 'ESCA, Atomic, Molecular and Solid State Structure Studied by Means of Electron Spectroscopy', Royal Society of Science of Uppsala (1965).
23. A.S. Baranski and W.R. Fawcett, *J. Electrochem. Soc.* **131** (1984) 2509.